

**Fates of secondary organic aerosols in the atmosphere identified from  
compound-specific dual-carbon isotope analysis of oxalic acid**

Buqing Xu<sup>1,2</sup>, Jiao Tang<sup>1,2</sup>, Tiangang Tang<sup>1,3</sup>, Shizhen Zhao<sup>1,2</sup>, Guangcai Zhong<sup>1,2</sup>,  
Sanyuan Zhu<sup>1,2</sup>, Jun Li<sup>1,2</sup>, Gan Zhang<sup>1,2\*</sup>

<sup>1</sup>State Key Laboratory of Organic Geochemistry, Guangzhou Institute of Geochemistry,  
Chinese Academy of Sciences, Guangzhou 510640, China.

<sup>2</sup>CAS Center for Excellence in Deep Earth Science, Guangzhou 510640, China

<sup>3</sup>Key Laboratory of Agro-ecological Processes in Subtropical Region, Institute of  
Subtropical Agriculture, Chinese Academy of Sciences, Changsha, 410125, China.

\*Correspondence: Gan Zhang ([zhanggan@gig.ac.cn](mailto:zhanggan@gig.ac.cn))

## 1 **Abstract**

2 Secondary organic aerosols (SOAs) are important components of fine particulates in  
3 the atmosphere. However, the sources of SOA precursor and atmospheric processes  
4 affecting SOAs are poorly understood. This limits our abilities to improve air quality  
5 and model aerosol-mediated climate forcing. Here, we use novel compound-specific  
6 dual-carbon isotope fingerprints ( $\Delta^{14}\text{C}$  and  $\delta^{13}\text{C}$ ) for individual SOA tracer molecule  
7 (i.e., oxalic acid) to investigate the fates of SOAs in the atmosphere at five emission  
8 hotspots in China. Coal combustion and vehicle exhausts accounted for ~55% of the  
9 sources of carbon in oxalic acid in Beijing and Shanghai, but biomass-burning and  
10 biogenic emissions accounted for ~70% of the sources of carbon in oxalic acid in  
11 Chengdu, Guangzhou, and Wuhan during the sampling period. The dual-carbon isotope  
12 signatures of oxalic acid and bulk organic carbon pools (e.g., water-soluble organic  
13 carbon) were compared to investigate the fates of SOAs in the atmosphere.  
14 Photochemical aging and aqueous-phase chemical processes dominant the formation of  
15 oxalic acid in summer and in winter, respectively. The results indicated that SOA carbon  
16 sources and chemical processes producing SOAs vary spatially and seasonally and  
17 these variations need to be included in Chinese climate projection models and air  
18 quality management practices.

## 19 **1. Introduction**

20 Great efforts have been made to decrease fine particle (PM<sub>2.5</sub>) pollution in China,  
21 which led to a great improvement in air quality during the last decade. However, PM<sub>2.5</sub>  
22 concentrations in Chinese urban areas are still much higher than the World Health  
23 Organization guideline (Xing et al., 2020). Further improvements in air quality will be  
24 difficult to achieve because primary particulate emissions have already been effectively  
25 controlled through stringent regulatory polices established since 2005 (Zhao et al., 2018)  
26 and emissions of volatile organic compounds have remained stable (Wang et al., 2021).  
27 Field observations have indicated that most organic aerosols in Chinese urban areas are  
28 secondary organic aerosols (SOAs) formed through oxidation of biogenic and  
29 anthropogenic precursor volatile organic compounds in the atmosphere (Huang et al.,  
30 2014). Our poor understanding of SOAs leads to some of the most important  
31 uncertainties when assessing global/regional climate forcing, either directly through  
32 solar radiation scattering and absorption or indirectly through aerosol–cloud  
33 interactions (Carlton et al., 2009; Hallquist et al., 2009). The sources of SOAs and  
34 chemical processes affecting SOAs in polluted areas of China need to be better  
35 understood to allow air quality control strategies to be optimized and accurate  
36 simulations of climate forcing to be developed.

37 The large variety of SOA precursors and the complexity of physical/chemical  
38 processes in real atmosphere renders great challenges in understanding SOA formation.  
39 Radiocarbon ( $\Delta^{14}\text{C}$ ) measurements of organic aerosol components allow high-precision  
40 fingerprinting to be achieved and the relative contributions of fossil fuels and  
41 biogenic/biomass sources to be determined (Gustafsson et al., 2009; Zhang et al., 2021).  
42 The  $\Delta^{14}\text{C}$  values for bulk organic aerosol materials such as black carbon (BC), organic  
43 carbon (OC), and water-soluble organic carbon (WSOC) have been determined  
44 (Andersson et al., 2015; Szidat et al., 2004; Szidat et al., 2006; Kirillova et al., 2013;  
45 Liu et al., 2014), but it is still difficult to directly measure the  $\Delta^{14}\text{C}$  values of SOAs in

46 atmospheric aerosols, which are chemically complex. Molecular-level  $\Delta^{14}\text{C}$  analysis of  
47 SOA markers can overcome this problem and remove uncertainty caused by using  
48 bottom-up organic precursor emission inventories (Chang et al., 2022).

49 Oxalic acid is a useful SOA marker because it is a key end-product of various  
50 transformation pathways in the atmosphere and is typically the most abundant SOA  
51 component (Boreddy and Kawamura, 2018; Kawamura and Bikkina, 2016;  
52 Myriokefalitakis et al., 2011). Stable carbon isotope measurements ( $\delta^{13}\text{C}$ ) of oxalic acid  
53 have been widely used to differentiate between various atmospheric processes affecting  
54 organic aerosols (Aggarwal and Kawamura, 2008; Wang et al., 2020; Zhang et al., 2016;  
55 Shen et al., 2022; Qi et al., 2022). Estimated kinetic isotope effects indicate that  
56 secondary formation and photochemical aging will affect  $\delta^{13}\text{C}$  in opposite ways  
57 (Kirillova et al., 2013). Combining  $\delta^{13}\text{C}$  and  $\Delta^{14}\text{C}$  measurements of oxalic acid could  
58 therefore allow the carbon sources of SOAs to be identified and processes affecting  
59 SOAs in the ambient atmosphere to be investigated.

60 In this study, we determined the dual-carbon isotope fingerprints ( $\Delta^{14}\text{C}$  and  $\delta^{13}\text{C}$ )  
61 of water-soluble SOA components (oxalic acid and related polar organic acids) and their  
62 parent water-soluble aerosols (i.e., WSOC) in five highly industrialized and populated  
63 megacities in China. The cities were Beijing, Chengdu, Guangzhou, Shanghai, and  
64 Wuhan, which were used to represent the five main regional carbon emission hotspots  
65 in China (the North China Plain, the Sichuan Basin, the Pearl River Delta, the Yangtze  
66 River Delta, and the middle reaches of the Yangtze River, respectively) (Fig. S1). We  
67 determined spatial and seasonal variations in the sources of carbon in oxalic acid in the  
68 study areas. We then compared the  $\delta^{13}\text{C}$  and  $\Delta^{14}\text{C}$  data for oxalic acid and the bulk  
69 organic aerosol pool to investigate the atmospheric processes affecting SOAs in the  
70 different cities and seasons. The molecular-level isotope fingerprints allowed  
71 observational constraints on the sources of carbon in SOAs and atmospheric processes  
72 affecting SOAs to be determined. The results improve our understanding of the fates of  
73 SOAs in the atmosphere.

## 74 **2 Methods**

### 75 **2.1 Sampling campaign**

76 Field sampling was performed in five megacities, Beijing, Chengdu, Guangzhou,  
77 Shanghai, and Wuhan. The locations of the cities are shown in [Fig. S1](#). Sampling was  
78 performed at an urban site and a suburban site in each city so that city-level data were  
79 acquired. The sampling campaign was described previously (Zhao et al., 2021) and  
80 sampling information is shown in [Table S1](#). At each site, PM<sub>2.5</sub> samples were collected  
81 onto pre-combusted Whatman quartz-fiber filters (20 cm × 25 cm) using a high-volume  
82 sampler and a flow rate of 1 m<sup>3</sup> min<sup>-1</sup>. Two intensive sampling campaigns were  
83 performed at each sampling site, with consecutive 24 h samples collected for 1 week in  
84 January 2018 (winter) and July 2018 (summer). A single sample representing the winter  
85 or summer at a sampling site was prepared by combining a one-tenth portion of each  
86 filter collected in a sampling campaign at the site. A total of 20 pooled samples were  
87 prepared and used in the subsequent experiments. One field blank sample for each site  
88 was collected and analyzed. The samples were stored at -20 °C until they were analyzed.

### 89 **2.2 Extracting water-soluble ions, WSOC, and dicarboxylic acids**

90 Each pooled sample was extracted four times. Each extraction involved adding 50  
91 mL of ultrapure water to the sample and ultrasonicing the sample for 30 min. The  
92 extracts were combined and passed through a 0.22 μm polytetrafluoroethylene  
93 membrane filter. Each extract was divided into several portions of different volumes,  
94 and the different portions were analyzed to determine the concentrations and/or carbon  
95 isotope compositions of water-soluble ions, WSOC, and dicarboxylic acids.

96 The carbon content of the WSOC was determined using a TOC-VCPH total  
97 organic carbon analyzer (Shimadzu, Kyoto, Japan) following the non-purgeable organic  
98 carbon analysis method (Kirillova et al., 2010). Water-soluble inorganic ions (Ca<sup>2+</sup>, Cl<sup>-</sup>,  
99 K<sup>+</sup>, Mg<sup>2+</sup>, Na<sup>+</sup>, NH<sub>4</sub><sup>+</sup>, NO<sub>3</sub><sup>-</sup>, and SO<sub>4</sub><sup>2-</sup>) were determined using a Metrohm 761  
100 Compact IC ion chromatograph (Metrohm, Herisau, Switzerland). The WSOC and

101 water-soluble inorganic ion concentrations in duplicate samples were determined, and  
102 the concentrations were corrected for the concentrations in the field blanks (Mo et al.,  
103 2021).

### 104 **2.3 Dicarboxylic acid analysis and carbon isotope analysis**

105 The stable carbon isotope  $\delta^{13}\text{C}$  and radiocarbon  $\Delta^{14}\text{C}$  values for dicarboxylic acids  
106 were determined using previously published methods (Xu et al., 2021). Briefly, an  
107 ultrapure water extract of a sample was evaporated to dryness and then derivatized with  
108 10%  $\text{BF}_3$  in 1-butanol (Sigma-Aldrich, St Louis, MO, USA) at 100 °C for 1 h to convert  
109 carboxyl groups into butyl ester groups. The derivatives were extracted with *n*-hexane  
110 and quantified by gas chromatography mass spectrometry before isotope analysis was  
111 performed. The  $\delta^{13}\text{C}$  values for individual diacids were determined by gas  
112 chromatography isotope ratio mass spectrometry (Thermo Fisher Scientific Delta V,  
113 Waltham, MA, USA). Each sample was analyzed in triplicate and the analytical errors  
114 for the replicate analyses were generally <0.3‰.

115 Compound-specific radiocarbon analysis of oxalic acid was achieved by  
116 separating and harvesting single compounds using a preparative capillary gas  
117 chromatograph in sufficient amounts to allow offline natural abundance  $^{14}\text{C}$   
118 measurements to be made by accelerator mass spectrometry. The preparative capillary  
119 gas chromatography isolates were rinsed with dichloromethane, completely dried, and  
120 combusted at 920 °C with CuO and Ag in a quartz tube to give  $\text{CO}_2$ . The  $\text{CO}_2$  was  
121 purified in a vacuum system and then reduced to graphite using the hydrogen reduction  
122 method. The  $\Delta^{14}\text{C}$  value was determined using the 1.5 SDH-1, 0.5 MV compact  
123 accelerator mass spectrometry facility (NEC, National Electrostatics Corporation, USA)  
124 at the Guangzhou Institute of Geochemistry of the Chinese Academy of Sciences (Zhu  
125 et al., 2015). Each accelerator mass spectrometry analysis  $^{14}\text{C}$  result is reported as a  
126 fraction modern ( $F_m$ ) normalized to a common  $\delta^{13}\text{C}$  values of -25‰. The results were  
127 corrected for background carbon using an isotope dilution method described in previous  
128 publications (Xu et al., 2021). The  $\delta^{13}\text{C}$  and  $F_m$  values for individual diacids were

129 calculated using the relevant isotope ratios for diacid derivatives and 1-butanol using  
130 an isotope mass balance equation. Each  $F_m$  result was converted into a “fraction of  
131 contemporary carbon” ( $F_c$ ) by normalizing the  $F_m$  using a conversion factor of 1.06 to  
132 correct for excess  $^{14}\text{C}$  from nuclear bomb tests (Xu et al., 2022).

## 133 **2.4 Carbon isotope analysis of WSOC**

134 A ~15 mL aliquot of a WSOC extract was cooled to  $-20\text{ }^\circ\text{C}$  and dried in a vacuum  
135 freeze drier. The residue was redissolved in ~200  $\mu\text{L}$  of ultrapure water, then 50  $\mu\text{L}$  was  
136 transferred to a tin capsule for stable carbon isotope analysis and 150  $\mu\text{L}$  was transferred  
137 to a capsule for radiocarbon analysis. The samples in the capsules were evaporated to  
138 dryness at  $60\text{ }^\circ\text{C}$  before isotope analyses were performed.

139 The carbon isotopes in the WSOC were determined using a previously published  
140 procedure (Mo et al., 2021). The  $\delta^{13}\text{C}$  value for WSOC was determined using a Flash  
141 2000 elemental analyzer connected to a Delta V ion ratio mass spectrometer (Thermo  
142 Fisher Scientific, Waltham, MA, USA). The  $\Delta^{14}\text{C}$  values for the WSOC samples were  
143 determined at the accelerator mass spectrometry facility (1.5 SDH-1, 0.5 MV, NEC,  
144 USA). Generally,  $>200\text{ }\mu\text{g}$  of WSOC were combusted and converted into graphite for  
145 each radiocarbon analysis.

## 146 **3 Results and Discussion**

### 147 **3.1 Spatiotemporal variations in dicarboxylic acids**

148 **Dicarboxylic acids, oxocarboxylic acids, and  $\alpha$ -dicarbonyls** concentrations in the  
149  $\text{PM}_{2.5}$  samples collected in the winter and summer in the five megacities were  
150 determined, and a total of 29 water-soluble organic species were identified, as shown  
151 in [Table S2](#). The diacid and related compound concentrations were slightly higher at  
152 the urban than suburban sites, but the differences were not significant. For each city,  
153 the mean of the concentrations found at the urban and suburban sites is therefore  
154 presented.

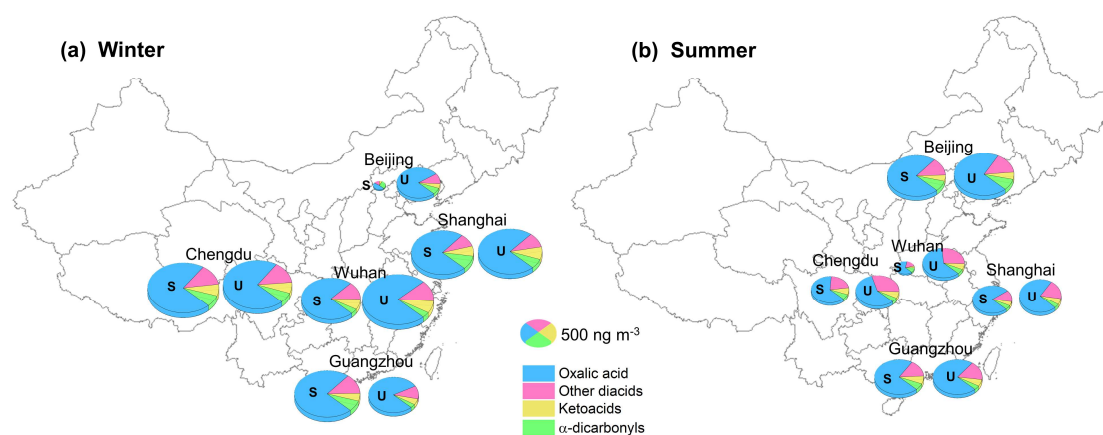
155 The total diacid concentrations in the samples from the five megacities were 25–

156 1300 ng m<sup>-3</sup> (mean ± standard deviation 690 ± 360 ng m<sup>-3</sup>), which were similar to  
157 concentrations previously found in other Asian megacities such as Chennai (mean 610  
158 ng m<sup>-3</sup>) (Pavuluri et al., 2010) and Hong Kong (mean 690 ng m<sup>-3</sup>) (Ho et al., 2006) and  
159 slightly lower than concentrations found in 14 Chinese cities in 2003 (890 ± 460 ng  
160 m<sup>-3</sup>) (Ho et al., 2007). Oxalic acid was the most abundant diacid at all of the sampling  
161 sites and contributed 70%–89% (mean 82%) of the total diacid concentrations. The  
162 mean oxalic acid to total diacid concentration ratios were significantly higher than the  
163 mean of 58% found for 14 urban sites in China in 2003 (Ho et al., 2007). The increase  
164 in the oxalic acid to total diacid concentration ratio between 2003 and 2018 indicated  
165 that secondary organic aerosol production in China increased between 2003 and 2018  
166 because oxalic acid is an end-product of the oxidation of many precursors (Ervens et  
167 al., 2011; Carlton et al., 2007; Lim et al., 2010; Lim et al., 2013). Malonic acid and  
168 succinic acid were approximately equally the second most abundant diacids,  
169 contributing 4.4% and 4.7%, respectively, of the total diacid concentrations, and  
170 phthalic acid, terephthalic acid, adipic acid, and azelaic acid were the next most  
171 abundant diacids. The mean oxoacid concentration was 54 ± 34 ng m<sup>-3</sup>, and glyoxylic  
172 acid and pyruvic acid were the most and second most abundant oxoacids, respectively.  
173 Two α-dicarbonyls (important oxalic acid precursors) were also determined (Fu et al.,  
174 2008; Warneck, 2003). Methylglyoxal was more abundant than glyoxal, and this was  
175 partly attributed to the rate of oxidation by OH radicals being lower for methylglyoxal  
176 than glyoxal (Meng et al., 2018).

177 In Beijing (in North China), the diacid concentration was markedly lower in winter  
178 (260 ng m<sup>-3</sup>) than summer (850 ng m<sup>-3</sup>) (Fig. 1), probably because weaker solar  
179 radiation and lower temperatures caused less photochemical oxidation to occur in  
180 winter than summer (Ho et al., 2007). In particular, during the winter sampling period,  
181 clean air masses originating in Siberia dominated the atmosphere in Beijing (Fig. S2)  
182 and may have caused the secondary aerosol precursor concentrations to be very low. In  
183 contrast, the winter to summer diacid concentration ratios for the cities in South China



184 (Chengdu, Guangzhou, Shanghai, and Wuhan) were >1 (range 1.4–4.2) (Fig. 1). Unlike  
 185 for Beijing, strong photochemical oxidation would have occurred in winter in the cities  
 186 in South China (Ho et al., 2007). The diacid concentrations were probably higher in  
 187 winter than summer because the mixing heights were lower and precipitation was less  
 188 frequent in winter than summer. Oxocarboxylic acids and  $\alpha$ -dicarbonyls had similar  
 189 spatial and seasonal patterns to diacids, the concentrations being higher in South China  
 190 in winter than summer but higher in North China in summer than winter.



191  
 192 **Figure 1.** Dicarboxylic acid, oxocarboxylic acid, and  $\alpha$ -dicarbonyl concentrations in  
 193 PM<sub>2.5</sub> collected in five Chinese megacities in (a) winter and (b) summer. Samples were  
 194 collected at a suburban site (S) and an urban site (U) in each city.

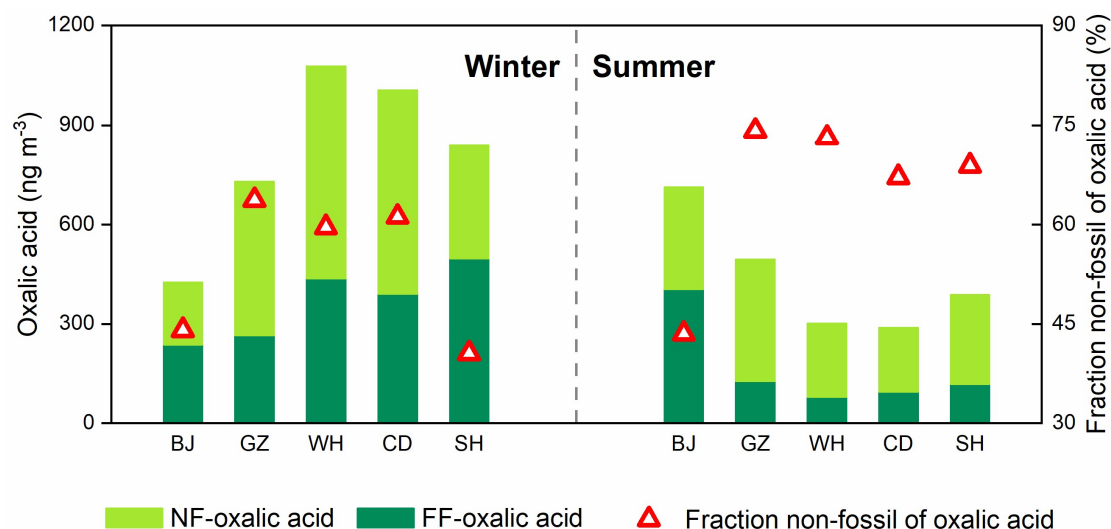
### 195 3.2 Radiocarbon-based oxalic acid source apportionment

196 We determined the  $\Delta^{14}\text{C}$  values for oxalic acid (the most abundant diacid) in the  
 197 samples. The sources of oxalic acid were apportioned based on the  $\Delta^{14}\text{C}$  data, and the  
 198 non-fossil contributions to the oxalic acid concentrations ( $f_{\text{NF-oxalic acid}}$ ) were 40%–  
 199 76% (mean  $61\% \pm 11\%$ ), as shown in Table S3. The high proportion of  $f_{\text{NF-oxalic acid}}$   
 200 demonstrates that even in the heavily populated and industrialized areas of China, non-  
 201 fossil emissions are important and ubiquitous sources of oxalic acid. The important non-  
 202 fossil sources of oxalic acid may be seasonally produced biogenic precursors and  
 203 precursors emitted during biomass burning. The  $f_{\text{NF-oxalic acid}}$  values were higher for  
 204 the suburban sites than the urban areas except for Shanghai (Table S3). This is  
 205 consistent with larger amounts of fossil fuels being consumed in urban areas than

206 suburban areas. However, intraurban differences were not marked, so the  $\Delta^{14}\text{C}$ -based  
207 source apportionment results for the different cities were compared.

208 The mean  $f_{\text{NF}}$ -oxalic acid value was higher in summer ( $67\% \pm 10\%$ ) than winter  
209 ( $54\% \pm 11\%$ ), indicating that more emissions were caused by fossil fuel combustion  
210 and/or less biogenic emissions occurred in winter than summer. In winter, fossil-fuel-  
211 derived carbon contributed  $\sim 60\%$  of the carbon in oxalic acid in Beijing and Shanghai  
212 (Fig. 2) but  $<40\%$  of the carbon in oxalic acid in Chengdu, Guangzhou, and Wuhan.  
213 This agreed with the results of a previous study in which the sources of SOA during  
214 winter haze events were apportioned using two complementary bilinear receptor  
215 models and fossil sources were found to contribute 63%, 50%, and 35% of SOAs in  
216 Beijing, Shanghai, and Guangzhou, respectively (Huang et al., 2014). Oxalic acid was  
217 therefore a good surrogate for SOA.

218 In summer, a mean of  $71\% \pm 4\%$  of the oxalic acid in Chengdu, Guangzhou,  
219 Shanghai, and Wuhan (in South China) was derived from natural biomass (Fig. 2).  
220 However, a large proportion (56%) of the oxalic acid in Beijing (in North China) was  
221 derived from fossil carbon (Fig. 2). Biogenic precursors are expected to be more  
222 important in summer than winter, but fossil-fuel-derived carbon contributed most of the  
223 oxalic acid in Beijing in both summer and winter. Back trajectories indicated that the  
224 air masses in Beijing during the summer sampling periods mostly originated over the  
225 Beijing–North China Plain (Fig. S2), which is one of the most polluted parts of China  
226 (Andersson et al., 2015; Zhao et al., 2021).



227

228

229

230

231

**Figure 2.** Mass concentrations of oxalic acid derived from non-fossil sources (NF) and fossil fuel (FF) and the mean proportions of non-fossil oxalic acid found for Beijing (BJ), Guangzhou (GZ), Wuhan (WH), Chengdu (CD), and Shanghai (SH) in winter and summer.

232

233

234

235

236

237

238

239

240

241

The concentrations of oxalic acid derived from non-fossil sources and fossil fuel were 190–660 ng m<sup>-3</sup> (mean 370 ± 150 ng m<sup>-3</sup>) and 81–520 ng m<sup>-3</sup> (mean 260 ± 150 ng m<sup>-3</sup>), respectively (Fig. 2). In winter, the concentrations of oxalic acid derived from fossil fuel were higher in cities in South China than in Beijing. The concentrations of oxalic acid derived from fossil fuel were markedly lower in summer than winter in the cities in South China but higher in summer than winter in Beijing. In summer, the concentrations of oxalic acid derived from fossil fuel were three–five times higher in Beijing than in the cities in South China (Fig. 2). This would have been caused by seasonally dependent fossil fuel consumption and meteorological conditions, as discussed above.

242

243

244

245

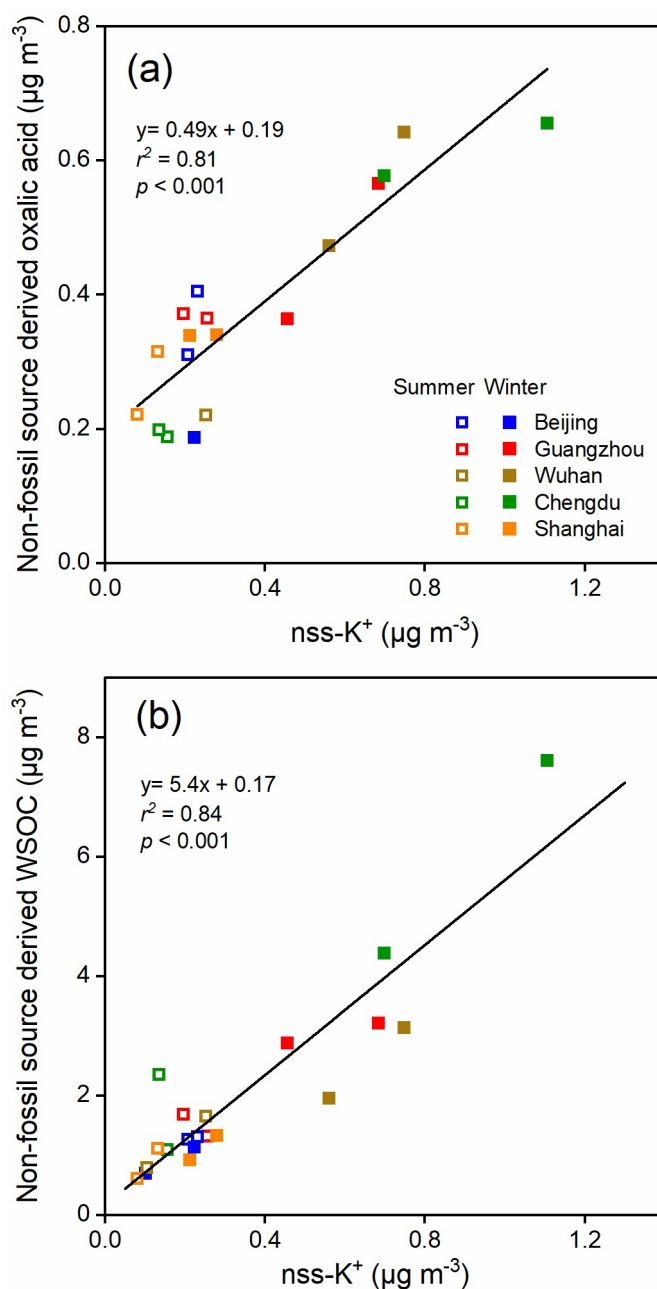
246

Oxalic acid derived from non-fossil sources made substantial contributions to or even dominated the oxalic acid in the cities we studied (Fig. 2). The concentrations of non-fossil oxalic acid in the cities in South China were higher in winter than summer. However, biogenic compounds (e.g., isoprene (Bikkina et al., 2014; Bikkina et al., 2021) and monoterpene (Link et al., 2021)) may contribute a smaller proportion of non-fossil

247 oxalic acid in winter than summer. The high non-fossil oxalic acid concentrations found  
248 in winter may therefore have been caused by local and regional biomass burning. As  
249 shown in Fig. 3a, the non-fossil oxalic acid concentrations positively correlated with  
250 the concentration of non-sea-salt potassium ( $\text{nss-K}^+$ ; a marker for biomass burning)  
251 ( $r^2=0.81$ ,  $p<0.001$ ), indicating that the high non-fossil oxalic acid concentrations were  
252 mainly caused by emissions of precursors through biomass burning. The slope of the  
253 regression line fitted to a plot of the non-fossil oxalic acid concentration against the  
254  $\text{nss-K}^+$  concentration ( $0.49 \pm 0.06$ ; Fig. 3a) was similar to the slope found in a previous  
255 study performed in the Pearl River Delta area in South China ( $0.55 \pm 0.08$ ) (Xu et al.,  
256 2022). When the biomass burning contribution was very low ( $\text{nss-K}^+=0 \mu\text{g m}^{-3}$ ), the  
257 mean non-fossil oxalic acid concentration ( $190 \text{ ng m}^{-3}$ ; Fig. 3a) was half of the mean  
258 total oxalic acid concentration ( $370 \text{ ng m}^{-3}$ ). This suggested that biogenic emissions  
259 and biomass burning contributed equally to the mean total oxalic acid concentration.

260 Non-fossil oxalic acid and  $\text{nss-K}^+$  were less abundant in all of the cities in summer  
261 than in winter (Fig. 3a), indicating that most of the non-fossil oxalic acid was produced  
262 through biogenic emissions in summer. On average, the non-fossil oxalic acid  
263 concentrations in Guangzhou, Wuhan, and Chengdu were 1.3, 2.5, and 3.2 times higher,  
264 respectively, in winter than summer (Fig. 3a), mostly because more biomass burning  
265 occurs in winter than summer. Less marked seasonal variations in non-fossil oxalic acid  
266 concentrations were found for Beijing and Shanghai (Fig. 3a), indicating that biomass  
267 burning may produce only a small proportion of the oxalic acid found in these cities.  
268 This is consistent with emission control legislation being stricter in Beijing and  
269 Shanghai than the other cities, meaning biomass burning activities (e.g., crop residue  
270 burning) are effectively controlled in Beijing and Shanghai (Qiu et al., 2016). The  
271 oxalic acid sources apportioned using the  $\Delta^{14}\text{C}$  data suggested that decreasing the  
272 concentrations of precursors derived from fossil fuels could be important for controlling  
273 SOA production in Beijing and Shanghai. In contrast, decreasing the concentrations of  
274 precursors derived from both fossil fuels and biomass combustion will be required to

275 decrease the SOA concentrations in areas such as Chengdu, Guangzhou, and Wuhan.



276

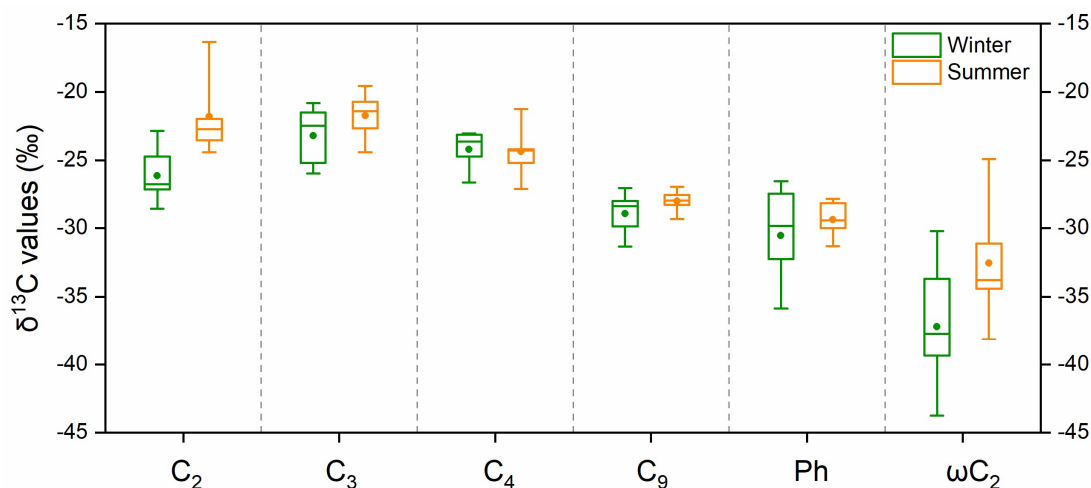
277 **Figure 3.** Relationships between (a) non-fossil-derived oxalic acid concentrations and  
278 non-sea-salt potassium (nss-K<sup>+</sup>) concentrations and between (b) non-fossil-derived  
279 water-soluble organic carbon (WSOC) concentrations and nss-K<sup>+</sup> concentrations.

### 280 3.3 Relationships between stable carbon isotope shifts and atmospheric processing

281 The stable carbon isotope composition ( $\delta^{13}\text{C}$ ) provides useful information about  
282 the sources of carbon and particularly about atmospheric processes affecting organic  
283 compounds. Primary emissions from various sources have different  $\delta^{13}\text{C}$  values. The

284  $\delta^{13}\text{C}$  value will change because of kinetic isotope effects during atmospheric processes  
285 (Kirillova et al., 2013) such as oxidation, secondary formation, oligomerization, and  
286 gas–particle partitioning (Bikkina et al., 2017b) in which lighter and heavier isotopes  
287 behave differently, although source mixing can also affect the  $\delta^{13}\text{C}$  value. The  $\delta^{13}\text{C}$   
288 values of diacids therefore have been used widely to track atmospheric processes and  
289 assess the degree of organic aerosol aging (Aggarwal and Kawamura, 2008; Zhang et  
290 al., 2016; Wang et al., 2020; Shen et al., 2022; Qi et al., 2022).

291 The  $\delta^{13}\text{C}$  values for the main diacids and oxoacids in the five cities that were  
292 studied are shown in Fig. 4 and Table S4. Oxalic acid had a markedly lower  $\delta^{13}\text{C}$  (by  
293 4.4‰) in winter than summer (Fig. 4). This would have been caused by differences in  
294 isotope fractionation caused by atmospheric processes in winter and summer,  
295 differences in oxalic acid sources in winter and summer, or a combination. The  $\delta^{13}\text{C}$   
296 values for the diacids with more carbon atoms ( $\text{C}_3 - \text{C}_9$  diacids) in winter and summer  
297 were not very (<1.5‰) different (Fig. 4), so differences in emission sources were not  
298 likely to be responsible for the marked seasonal differences in oxalic acid  $\delta^{13}\text{C}$  values.  
299 The  $\text{nss-SO}_4^{2-}$  to  $\text{SO}_4^{2-}$  ratio ( $97\% \pm 3\%$ ) and  $\text{nss-K}^+$  to  $\text{K}^+$  ratio ( $94\% \pm 4\%$ ) indicated  
300 that marine emissions with heavier  $\delta^{13}\text{C}$  signatures did not make marked contributions  
301 (Dasari et al., 2019) (Fig. S3), particularly in the coastal cities Guangzhou and Shanghai.  
302 The seasonal differences in the  $\delta^{13}\text{C}$  values could have been stronger for oxalic acid  
303 than diacids with more carbon atoms because processes involving isotope fractionation  
304 affected diacids with fewer carbon atoms more than diacids with more carbon atoms.  
305 The short-chain acid glyoxylic acid is an important precursor of oxalic acid (Bikkina et  
306 al., 2017a; Carlton et al., 2007; Lim et al., 2013) that also had markedly different  $\delta^{13}\text{C}$   
307 values (by 4.7‰) in winter and summer (Fig. 4). The clear seasonal differences in the  
308  $\delta^{13}\text{C}$  values for oxalic acid and glyoxylic acid suggested that atmospheric processes  
309 markedly affected oxalic acid and glyoxylic acid, which are small molecules.



310

311 **Figure 4.** Box-and-whisker plot of the  $\delta^{13}\text{C}$  values for four saturated aliphatic  
 312 dicarboxylic acids (C<sub>2</sub>, C<sub>3</sub>, C<sub>4</sub>, and C<sub>9</sub>), phthalic acid (Ph), and glyoxylic acid ( $\omega\text{C}_2$ ) in  
 313 PM<sub>2.5</sub> collected in five Chinese megacities in January 2018 (winter) and July 2018  
 314 (summer). Each box indicates the median (the line within the box), the mean (the solid  
 315 dot within the box), the interquartile range (the ends of the box), and the 10th and 90th  
 316 percentiles (the whiskers).

317 Oxalic acid can be emitted from primary sources, but most oxalic acid in  
 318 atmospheric aerosol is formed through aqueous-phase reactions and/or photochemical  
 319 aging, i.e., secondary sources (Huang and Yu, 2007; Van Pinxteren et al., 2014; Xu et  
 320 al., 2022). During aqueous-phase reactions, the reactivity of isotopically lighter carbon  
 321 (<sup>12</sup>C) is higher compared to that of isotopically heavier carbon (<sup>13</sup>C), and this will cause  
 322 the  $\delta^{13}\text{C}$  values to be lower for the particulate products than the gaseous reactants  
 323 (Anderson et al., 2004; Fisseha et al., 2009; Irei et al., 2006). In contrast, photochemical  
 324 aging processes can give gaseous products (e.g., CO<sub>2</sub>, CO, and volatile organic  
 325 compounds) which will be enriched in lighter isotopes, causing  $\delta^{13}\text{C}$  to be higher for  
 326 the residual (aged) aerosols than the gaseous oxidation products (Aggarwal and  
 327 Kawamura, 2008; Pavuluri and Kawamura, 2012).

328 It has been found in several previous studies that aqueous-phase processes play  
 329 important roles in SOA formation in China in winter (Gkatzelis et al., 2021; Lv et al.,  
 330 2022; Yu et al., 2021; Wang et al., 2021). This was largely caused by the growth of

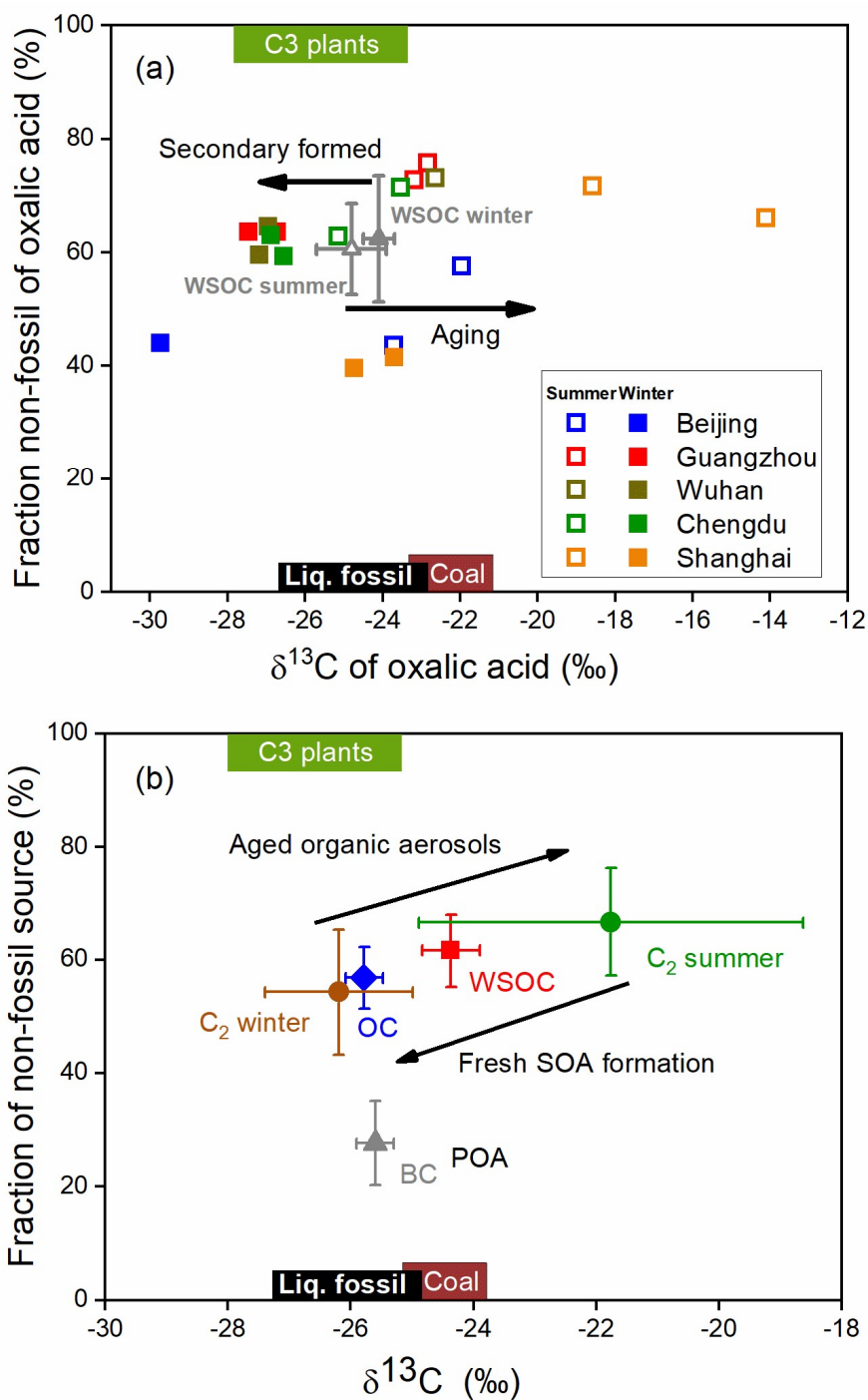
331 aerosol liquid water content (ALWC), because the hygroscopic particles were abundant  
332 in winter (Yu et al., 2021; Wang et al., 2020; Chen et al., 2021). Ammonium, nitrate,  
333 and sulfate are the most important hygroscopic particles in areas with intense  
334 anthropogenic emissions (Wu et al., 2018; Lv et al., 2022). As shown in Table S5, the  
335 nitrate concentrations were nine times higher in winter than summer and the ammonium  
336 concentrations were 2.5 times higher in winter than summer. The inorganic aerosol  
337 ( $\text{Ca}^{2+}$ ,  $\text{Cl}^-$ ,  $\text{K}^+$ ,  $\text{Mg}^{2+}$ ,  $\text{Na}^+$ ,  $\text{NH}_4^+$ ,  $\text{NO}_3^-$ , and  $\text{SO}_4^{2-}$ ) contents and meteorological  
338 parameters (temperature and relative humidity) were used in the ISORROPIA-II  
339 thermodynamic model (Xu et al., 2022) and the results indicated that the ALWCs in all  
340 five cities were markedly higher in winter ( $60 \pm 76 \mu\text{g m}^{-3}$ ) than summer ( $8.5 \pm 5.1 \mu\text{g}$   
341  $\text{m}^{-3}$ ) (Table S5). The increase in ALWC in winter may facilitate the partitioning of  
342 water-soluble organic precursors to the aqueous phase of the aerosol and promote the  
343 subsequent formation of low volatile compounds such as oxalic acid in the aqueous  
344 phase. Meanwhile, aerosols will be less aged in winter than summer because the  
345 temperature is lower and less solar radiation is present in winter than summer.  
346 Assuming that source mixing made a minor contribution, the atmospheric processes  
347 aging and aqueous SOA formation would have strongly contributed to seasonal  
348 variations in the  $\delta^{13}\text{C}$  values for oxalic acid in the five Chinese megacities that were  
349 studied.

#### 350 **3.4 Tracing sources and aerosol processing using the $\delta^{13}\text{C}$ and $\Delta^{14}\text{C}$ values**

351 Aerosol sources and atmospheric processes affecting aerosols were investigated  
352 using the  $\delta^{13}\text{C}$  and  $\Delta^{14}\text{C}$  values for oxalic acid, as shown in Fig. 5a. As shown in Fig.  
353 5a, the  $\delta^{13}\text{C}$  value was higher and the  $\Delta^{14}\text{C}$  value indicated more biogenic oxalic acid  
354 was present in summer than winter. The oxalic acid data for Chengdu, Guangzhou, and  
355 Wuhan strongly overlap in the plot, suggesting that oxalic acid in these cities had similar  
356 sources and had been subjected to similar processes. In contrast, the  $\delta^{13}\text{C}$  and  $\Delta^{14}\text{C}$   
357 values for oxalic acid in Beijing and Shanghai are spread over a large area in the plot,  
358 indicating that oxalic acid in these cities had various sources and had been subjected to



359 various atmospheric processes. The fossil-carbon contributions to oxalic acid were  
 360 markedly higher in Beijing and Shanghai than the other cities, as described above.  
 361 However, the  $\delta^{13}\text{C}$  values were lower in Beijing and higher in Shanghai. The  $\delta^{13}\text{C}$   
 362 values suggested that organic aerosols in Beijing were predominantly fresh SOAs but  
 363 that organic aerosols were more affected by photochemical aging in Shanghai than the  
 364 other cities.



365

366 **Figure 5.**  $^{14}\text{C}$ -based non-fossil source fractions plotted against the  $\delta^{13}\text{C}$  values for  
367 molecules and carbonaceous aerosol components. **(a)** Aerosol oxalic acid collected in  
368 Beijing (blue), Guangzhou (red), Wuhan (brown), Chengdu (green), and Shanghai  
369 (orange) in summer (open squares) and winter (filled squares). The mean dual carbon  
370 isotope signals for water-soluble organic carbon (WSOC) in the five cities in summer  
371 (gray open triangles) and winter (gray filled triangles) are also shown (Fig. S4). Each  
372 error bar indicates the standard deviation. **(b)** Annual mean values for black carbon (BC,  
373 gray triangles), organic carbon (OC, blue diamonds), WSOC (red squares), and oxalic  
374 acid ( $\text{C}_2$ , brown and green circles) in the five cities (see Table 1 for detailed data and  
375 references). Each error bar indicates the standard deviation. Here POA and SOA refer  
376 to primary organic aerosol and secondary organic aerosol, respectively. The expected  
377 dual carbon signatures for coal, liquid fossil carbon, and C3 plants were taken from  
378 previous publications (Widory et al., 2004; Huang et al., 2006; Kawashima and  
379 Haneishi, 2012; Smith and Epstein, 1971; Martinelli et al., 2002; Cao et al., 2011).

380 The mean dual carbon isotope signals for WSOC pool in the five cities were  
381 determined and are shown as gray triangles in Fig. 5a for comparison with the signals  
382 for oxalic acid. The aging process is more important in summer than winter, but the  
383 mean  $\delta^{13}\text{C}$  values for WSOC in summer ( $-24.8\text{‰} \pm 0.9\text{‰}$ ) and winter ( $-24.1\text{‰} \pm 0.4\text{‰}$ )  
384 were not markedly different (Fig. S4). The  $\Delta^{14}\text{C}$  data for WSOC indicated that the mean  
385 non-fossil-carbon contribution to WSOC was  $62\% \pm 10\%$  (range 45%–80%; Fig. S4),  
386 which was similar to the contribution in 10 Chinese cities in 2013 (mean  $60\% \pm 9\%$ ,  
387 range 38%–81%) (Mo et al., 2021). The WSOC concentration was almost twice as high  
388 in winter than summer, but the non-fossil-carbon contributions to WSOC in winter and  
389 summer were similar ( $61\% \pm 11\%$  in winter versus  $60\% \pm 9\%$  in summer, Fig. 5a). As  
390 shown in Fig. 3b, the non-fossil WSOC concentration significantly correlated with the  
391 biomass burning marker (nss- $\text{K}^+$ ) concentration ( $r^2=0.84$ ,  $p<0.001$ ). When the biomass  
392 burning contribution was very low (nss- $\text{K}^+ \approx 0 \mu\text{g m}^{-3}$ ), the non-fossil WSOC  
393 concentration was close to  $0 \mu\text{g m}^{-3}$  (Fig. 3b). Unlike oxalic acid, for which biogenic

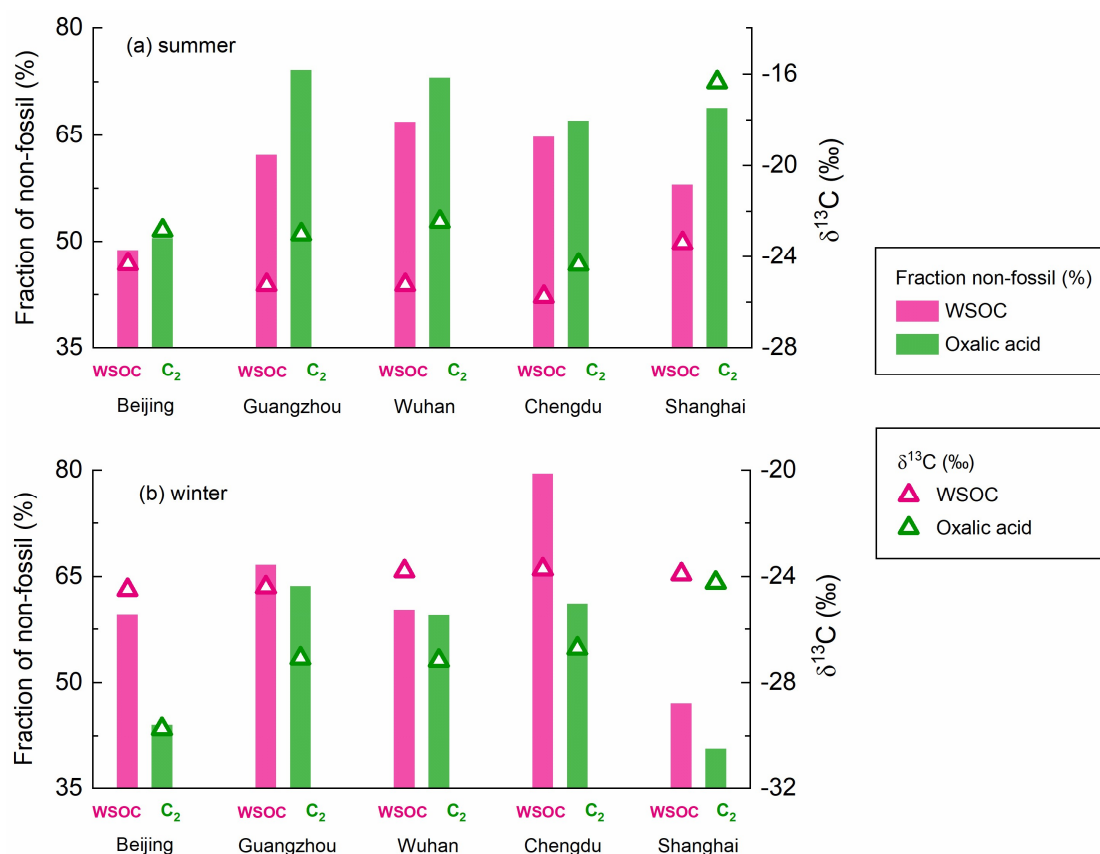
394 emissions and biomass burning were equally important sources, most of the non-fossil  
395 WSOC was associated with biomass burning. The similar WSOC source patterns in  
396 winter and summer were therefore probably caused by fossil fuel combustion and  
397 biomass-burning emissions having similar seasonal variations.

398 As mentioned above, the average  $\delta^{13}\text{C}$  and  $\Delta^{14}\text{C}$  values for WSOC remain almost  
399 stable between winter and summer (Fig. 5a), mainly because the source patterns of  
400 WSOC were similar in different seasons. Bulk aerosol pool such as WSOC consist both  
401 the reactants and products of the photochemical reactions. Therefore, the isotopic  
402 fractionation effects during atmospheric processes would introduce only minor changes  
403 in the  $\delta^{13}\text{C}$  values of WSOC. Oxalic acid contributed a mean of 5.5% (range  
404 1.4%–10.7%) of the WSOC concentration and was probably the most abundant  
405 compound (Myriokefalitakis et al., 2011). However, the carbon isotope compositions  
406 of oxalic acid were significantly different between winter and summer (Fig. 6). This  
407 suggested that oxalic acid could have different carbon sources and be affected by  
408 different atmospheric processes between winter and summer.

409 The  $\delta^{13}\text{C}$  values of oxalic acid were higher and the  $\Delta^{14}\text{C}$  values indicated more  
410 oxalic acid than WSOC was formed from non-fossil carbon in summer (Fig. 5a and Fig.  
411 6a). The  $\delta^{13}\text{C}$  value has been found to increase as the number of carbon atoms in diacids  
412 decreases (Aggarwal and Kawamura, 2008; Pavuluri et al., 2011), suggesting that  
413 shorter-chain diacids, which can form through photochemical aging of longer-chain  
414 diacids, will become enriched in  $^{13}\text{C}$  during aging. The  $\delta^{13}\text{C}$  values of WSOC pool  
415 would refer to both the reactants and products of the atmospheric processes. Enrichment  
416 of  $^{13}\text{C}$  in oxalic acid relative to WSOC (Fig. 6a) therefore probably reflected that oxalic  
417 acid was photochemical aging product (remaining reactant) in WSOC aerosols in  
418 summer. The  $\Delta^{14}\text{C}$  values indicated more oxalic acid than WSOC was formed from  
419 non-fossil carbon in summer (Fig. 6a). This could have been because fossil-carbon  
420 components are more recalcitrant than biomass and biogenic components of organic  
421 aerosols to oxidative aging (Elmquist et al., 2006; Kirillova et al., 2014b; Kirillova et

422 al., 2014a), meaning aged oxalic acid (with a higher  $\delta^{13}\text{C}$  value) will preferentially form  
423 from non-fossil carbon (with a higher  $\Delta^{14}\text{C}$  value). As discussed above, biogenic  
424 emissions made larger contributions of oxalic acid than WSOC in summer, which gave  
425 the same results.

426 In contrast, the  $\delta^{13}\text{C}$  values were lower and the  $\Delta^{14}\text{C}$  values indicated more oxalic  
427 acid than WSOC was formed from fossil carbon in winter (Fig. 5a and Fig. 6b). The  
428 lower  $\delta^{13}\text{C}$  values for oxalic acid found in winter suggested that oxalic acid indicates  
429 freshly formed SOA product in WSOC aerosols, as opposite to remaining reactant in  
430 summer. WSOC aerosols are mixtures of primary organic aerosols (e.g., sugars) and  
431 SOAs. Only a small fraction of water-soluble primary organic aerosols would have had  
432 fossil fuel sources (Liu et al., 2014; Mo et al., 2021). Therefore, a higher fossil-carbon  
433 contribution to water-soluble SOA than WSOC aerosol was expected, and this was  
434 indicated by the  $\Delta^{14}\text{C}$  values for oxalic acid indicating important fossil-carbon sources.  
435 It has been suggested that substantial fossil-carbon-derived precursors are probably  
436 oxidized to give water-soluble SOAs through aqueous-phase chemical processes,  
437 giving products such as oxalic acid with lower  $\delta^{13}\text{C}$  values and higher fossil-carbon  
438 contributions (Xu et al., 2022). Aqueous-phase processes are facilitated by a high  
439 ALWC, which is higher in winter than summer because the hygroscopic particle (e.g.,  
440 ammonia and nitrate) mass is higher in winter than summer (Lv et al., 2022; Xu et al.,  
441 2022) and meteorological conditions (e.g., the boundary layer height, temperature, and  
442 wind speed) are unfavorable in winter (Gkatzelis et al., 2021). Photochemical aging is  
443 suppressed in winter because of lower temperatures and weaker solar radiation than in  
444 summer. This means that more aqueous-phase production of fresh SOA than aerosol  
445 photochemical aging will occur in urban areas in China in winter.



446

447 **Figure 6.** Proportions of non-fossil sources (determined from the  $^{14}\text{C}$  values) and  $\delta^{13}\text{C}$   
 448 values for water-soluble organic carbon (WSOC) and oxalic acid ( $\text{C}_2$ ) in Beijing,  
 449 Guangzhou, Wuhan, Chengdu, and Shanghai in (a) summer and (b) winter.

### 450 3.5. Comparison with carbonaceous aerosol components

451 The  $\delta^{13}\text{C}$  and  $\Delta^{14}\text{C}$  values for oxalic acid were compared with the mean annual  
 452 isotope compositions of the bulk carbonaceous aerosols (i.e., BC, OC, and WSOC) in  
 453  $\text{PM}_{2.5}$  found in the five study areas in previous studies (Fig. 5b and Table 1). Non-fossil-  
 454 source-derived carbon was the dominant contributor of OC and WSOC aerosols, the  
 455 mean annual contributions being  $57\% \pm 5\%$  and  $62\% \pm 6\%$ , respectively (Fig. 5b). The  
 456 large contribution of non-fossil carbon to OC and WSOC (a sub-fraction of OC)  
 457 contrasted strongly with the large contribution of fossil carbon ( $72\% \pm 7\%$ ) to BC (Fig.  
 458 5b). This was probably because OC aerosols are more affected than BC by biogenic  
 459 emissions and biomass burning.

460 The  $\delta^{13}\text{C}$  values were higher and the  $\Delta^{14}\text{C}$  values indicated smaller contributions  
 461 of fossil carbon for WSOC than OC in both winter and summer (Fig. 5b). Similar results

462 have been found at other locations and for different aerosol sizes (Kirillova et al., 2013;  
 463 Kirillova et al., 2014a; Kirillova et al., 2014b; Bosch et al., 2014), and this was  
 464 explained by atmospheric aging affecting water-soluble organic aerosols more than  
 465 organic aerosols. SOA formation typically causes  $\delta^{13}\text{C}$  to decrease, so fresh secondary  
 466 production of WSOC from fossil carbon would be less likely. However, the sources and  
 467 processes affecting the different aerosol components were masked in the mean isotope  
 468 contents of the aerosol mixtures. Oxalic acid is one of the most abundant compounds  
 469 in WSOC aerosols. The  $\delta^{13}\text{C}$  values were lower for the oxalic acid than the WSOC and  
 470 the  $\Delta^{14}\text{C}$  values indicated that fossil carbon made larger contributions to the oxalic acid  
 471 than the WSOC aerosol in winter (Fig. 5b). The marked differences between the  
 472 different organic aerosol components indicated that dual-carbon-isotope studies of  
 473 more aerosol molecules and components should be performed to improve our  
 474 understanding of the origins and evolution of organic aerosols in the atmosphere.

475 **Table 1.** Compilation of literature values of  $\delta^{13}\text{C}$  compositions and  $^{14}\text{C}$ -based non-fossil  
 476 source fraction ( $f_{NF}$ ) for black carbon (BC), organic carbon (OC), water-soluble organic  
 477 carbon (WSOC), and oxalic acid in  $\text{PM}_{2.5}$  samples collected from Beijing, Shanghai,  
 478 Guangzhou, Chengdu, and Wuhan.

Components	Location	Season	$\delta^{13}\text{C}$ (‰)	$f_{NF}$ (%)	References
BC	Beijing	Annual	NA <sup>a</sup>	21	(Zhang et al., 2015)
	Beijing	Annual	NA	18	(Zhang et al., 2017)
	Beijing	Annual	-24.6	24	(Fang et al., 2018)
	Beijing	Summer/winter	-25.8	NA	(Cao et al., 2011)
	Shanghai	Summer/winter	-25.9	NA	(Cao et al., 2011)
	Shanghai	Annual	-25.6	30	(Fang et al., 2018)
	Guangzhou	Summer/winter	-25.9	NA	(Cao et al., 2011)
	Guangzhou	Annual	-25.3	25	(Fang et al., 2018)
	Chengdu	Annual	-26.1	41	(Fang et al., 2018)
	Wuhan	Summer/winter	-25.4	NA	(Cao et al., 2011)
	Wuhan	Winter	NA	26	(Liu et al., 2016b)
	Average		-25.6±0.3	28±7	
OC	Beijing	Summer/winter	-26.0	NA	(Cao et al., 2011)
	Beijing	Annual	NA	52	(Zhang et al., 2017)
	Beijing	Annual	NA	50	(Liu et al., 2020)
	Shanghai	Summer/winter	-25.8	NA	(Cao et al., 2011)
	Shanghai	Winter	NA	51	(Huang et al., 2014)

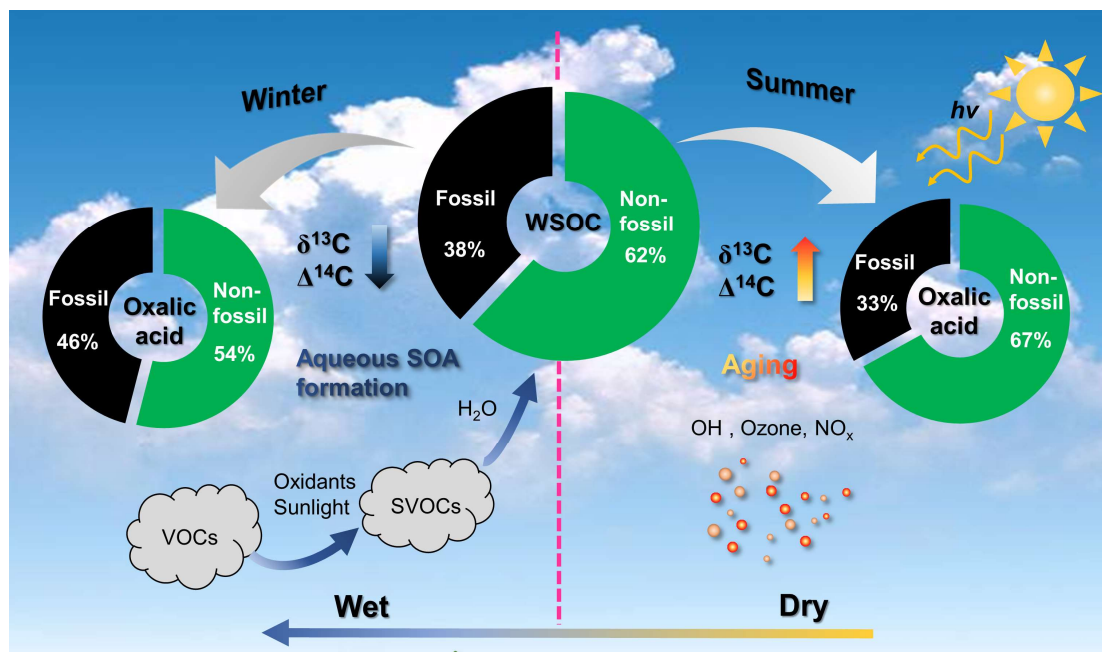
	Shanghai	Annual	NA	53	(Liu et al., 2020)
	Guangzhou	Summer/winter	-26	NA	(Cao et al., 2011)
	Guangzhou	Annual	NA	55	(Liu et al., 2020)
	Guangzhou	Spring	NA	54	(Liu et al., 2016a)
	Chengdu	autumn	NA	73	(Liu et al., 2017)
	Wuhan	Summer/winter	-25.6	NA	(Cao et al., 2011)
	Wuhan	Winter	NA	62	(Liu et al., 2016b)
	Wuhan	Autumn	NA	66	(Liu et al., 2017)
	Average		-25.9±0.3	57±5	
WSOC	Beijing	Summer/winter	-24.4	55	This work
	Shanghai	Summer/winter	-23.6	53	This work
	Guangzhou	Summer/winter	-24.8	63	This work
	Chengdu	Summer/winter	-24.7	72	This work
	Wuhan	Summer/winter	-23.6	65	This work
	Beijing	Annual	-23.7	56	(Mo et al., 2021)
	Shanghai	Annual	-24	58	(Mo et al., 2021)
	Guangzhou	Annual	-24.7	59	(Mo et al., 2021)
	Chengdu	Annual	-24.9	69	(Mo et al., 2021)
	Wuhan	Annual	-24.3	67	(Mo et al., 2021)
		Average		-24.4±0.5	62±6
Oxalic acid	Beijing	Summer	-22.8	50.5	This work
	Shanghai	Summer	-16.3	68.8	This work
	Guangzhou	Summer	-23	74.2	This work
	Chengdu	Summer	-24.3	67.1	This work
	Wuhan	Summer	-22.4	73.1	This work
	Beijing	Winter	-25.8	44.1	This work
	Shanghai	Winter	-24.2	40.6	This work
	Guangzhou	Winter	-27.1	63.7	This work
	Chengdu	Winter	-26.7	61.2	This work
	Wuhan	Winter	-27.1	62.1	This work
		Average	Summer	-21.8±3.1	67±10
	Average	Winter	-26.2±1.2	54±11	

479 <sup>a</sup> NA: no data

## 480 **4 Conclusions**

481 The  $\Delta^{14}\text{C}$  and  $\delta^{13}\text{C}$  values of oxalic acid in five megacities in China gave valuable  
482 information about the sources of carbon in SOAs and atmospheric processes affecting  
483 SOAs. The method allowed the fates of SOA in the atmosphere in urban areas to be  
484 investigated even though SOAs are very complex. The SOA sources apportioned from  
485 the  $^{14}\text{C}$  values indicated marked seasonal variations, non-fossil carbon being dominant  
486 in summer and fossil carbon and non-fossil carbon making similar contributions in  
487 winter. Precursors containing fossil carbon emitted through coal combustion or by

488 vehicles were mostly responsible for SOA formation in Beijing and Shanghai. SOA  
 489 formation was mainly associated with precursors containing non-fossil carbon emitted  
 490 through biomass burning and/or biogenic emissions in Chengdu, Guangzhou, and  
 491 Wuhan.



492  
 493 **Figure 7.** Schematic of the atmospheric fates of secondary organic aerosols (SOAs) in  
 494 winter and summer. VOCs means volatile organic compounds, SVOCs means semi-  
 495 volatile organic compounds, and WSOC means water-soluble organic carbon.

496 The dual-carbon-isotope datasets for the individual SOA molecules and bulk  
 497 organic aerosols indicated that there were two opposite seasonal organic aerosol  
 498 evolution processes. The fates of SOAs in the atmosphere in winter and summer are  
 499 shown in Fig. 7. In winter, the high hygroscopic particle mass and unfavorable  
 500 meteorological conditions (low temperature and high humidity) increase aerosol liquid  
 501 water formation, which causes fossil-derived water-soluble gaseous organic precursors  
 502 to dissolve in the aerosol liquid water and aqueous SOA to form (Fig. 7). Oxalic acid  
 503 indicates freshly formed aqueous SOA in winter because the  $\delta^{13}\text{C}$  values were lower  
 504 for oxalic acid than WSOC and the contribution of fossil carbon was higher for oxalic  
 505 acid than WSOC. In summer, organic aerosols are more affected by photochemical  
 506 aging than fresh SOA formation because of the high temperature and the high amount



507 of solar radiation present (Fig. 7). Oxalic acid was affected by SOA aging in summer  
508 and the  $\delta^{13}\text{C}$  and  $\Delta^{14}\text{C}$  values were higher for oxalic acid than WSOC.

509 In this study, one pooled sample was used to represent the winter or summer at a  
510 sampling site. Future compound-specific dual-carbon isotope studies covering a wide  
511 range of the temporal and spatial scale are strongly warranted to gain deeper insight  
512 into the fates of SOAs in China. Overall, we found that the carbon sources and SOA  
513 evolution processes were markedly different in different cities and seasons. There is a  
514 need to include the large spatial and seasonal variations in SOA fates (including  
515 precursor sources, SOA formation through gas-phase oxidation and from aqueous-  
516 phase chemicals, and SOA aging) in climate projection models and air quality  
517 management in China.

518 **Data availability.** The data underlying the findings of this study are available in this  
519 article and its Supplementary Information. The derived data generated in this research  
520 will be shared on reasonable request to the corresponding author (GZ).

521 **Author contributions.** GZ and BX designed the study. GCZ and SZZ provided the  
522 samples. BX, JT and SYZ carried out the measurements. BX processed data and wrote  
523 the paper. GZ, TT, and JL commented on the manuscript.

524 **Competing interests.** The authors declare no competing interests.

525 **Acknowledgements.** We thank Gareth Thomas, PhD, from Liwen Bianji (Edanz)  
526 (<https://www.liwenbianji.cn>), for editing the language of a draft of this manuscript.

527 **Financial support.** This work was funded by the Natural Science Foundation of China  
528 (42030715 and 42192510), the Alliance of International Science Organizations  
529 (ANSO-CR-KP-2021-05), the Natural Science Foundation of Guangdong Province,  
530 China (2017BT01Z134 and 2022A1515011679), and the China postdoctoral Science  
531 Foundation (2022M720143).

## 532 **References**

- 533 Aggarwal, S. G. and Kawamura, K.: Molecular distributions and stable carbon isotopic  
534 compositions of dicarboxylic acids and related compounds in aerosols from Sapporo, Japan:  
535 Implications for photochemical aging during long-range atmospheric transport, *J. Geophys.*  
536 *Res.: Atmos.*, 113, 10.1029/2007jd009365, 2008.
- 537 Anderson, R. S., Huang, L., Iannone, R., Thompson, A. E., and Rudolph, J.: Carbon Kinetic Isotope  
538 Effects in the Gas Phase Reactions of Light Alkanes and Ethene with the OH Radical at  $296 \pm$   
539  $4$  K, *J. Phys. Chem. A*, 108, 11537-11544, 10.1021/jp0472008, 2004.
- 540 Andersson, A., Deng, J., Du, K., Zheng, M., Yan, C., Skold, M., and Gustafsson, O.: Regionally-  
541 varying combustion sources of the January 2013 severe haze events over eastern China, *Environ.*  
542 *Sci. Technol.*, 49, 2038-2043, 10.1021/es503855e, 2015.
- 543 Bikkina, S., Kawamura, K., and Sarin, M.: Secondary organic aerosol formation over coastal ocean:  
544 inferences from atmospheric water-soluble low molecular weight organic compounds, *Environ.*  
545 *Sci. Technol.*, 51, 4347-4357, 10.1021/acs.est.6b05986, 2017a.
- 546 Bikkina, S., Kawamura, K., Miyazaki, Y., and Fu, P.: High abundances of oxalic, azelaic, and  
547 glyoxylic acids and methylglyoxal in the open ocean with high biological activity: Implication

548 for secondary OA formation from isoprene, *Geophys. Res. Lett.*, 41, 3649-3657,  
549 10.1002/2014gl059913, 2014.

550 Bikkina, S., Kawamura, K., Sakamoto, Y., and Hirokawa, J.: Low molecular weight dicarboxylic  
551 acids, oxocarboxylic acids and  $\alpha$ -dicarbonyls as ozonolysis products of isoprene: Implication  
552 for the gaseous-phase formation of secondary organic aerosols, *Sci. Total Environ.*, 769, 144472,  
553 <https://doi.org/10.1016/j.scitotenv.2020.144472>, 2021.

554 Bikkina, S., Andersson, A., Ram, K., Sarin, M. M., Sheesley, R. J., Kirillova, E. N., Rengarajan, R.,  
555 Sudheer, A. K., and Gustafsson, Ö.: Carbon isotope-constrained seasonality of carbonaceous  
556 aerosol sources from an urban location (Kanpur) in the Indo-Gangetic Plain, *J. Geophys. Res.:*  
557 *Atmos.*, 122, 4903-4923, 10.1002/2016jd025634, 2017b.

558 Boreddy, S. K. R. and Kawamura, K.: Investigation on the hygroscopicity of oxalic acid and  
559 atmospherically relevant oxalate salts under sub- and supersaturated conditions, *Environ. Sci.:*  
560 *Processes Impacts*, 20, 1069-1080, 10.1039/c8em00053k, 2018.

561 Bosch, C., Andersson, A., Kirillova, E. N., Budhavant, K., Tiwari, S., Praveen, P. S., Russell, L. M.,  
562 Beres, N. D., Ramanathan, V., and Gustafsson, Ö.: Source-diagnostic dual-isotope composition  
563 and optical properties of water-soluble organic carbon and elemental carbon in the South Asian  
564 outflow intercepted over the Indian Ocean, *J. Geophys. Res.: Atmos.*, 119, 11,743-711,759,  
565 10.1002/2014jd022127, 2014.

566 Cao, J.-j., Chow, J. C., Tao, J., Lee, S.-c., Watson, J. G., Ho, K.-f., Wang, G.-h., Zhu, C.-s., and Han,  
567 Y.-m.: Stable carbon isotopes in aerosols from Chinese cities: Influence of fossil fuels, *Atmos.*  
568 *Environ.*, 45, 1359-1363, <https://doi.org/10.1016/j.atmosenv.2010.10.056>, 2011.

569 Carlton, A. G., Wiedinmyer, C., and Kroll, J. H.: A review of Secondary Organic Aerosol (SOA)  
570 formation from isoprene, *Atmos. Chem. Phys.*, 9, 4987-5005, 10.5194/acpd-9-8261-2009, 2009.

571 Carlton, A. G., Turpin, B. J., Altieri, K. E., Seitzinger, S., Reff, A., Lim, H.-J., and Ervens, B.:  
572 Atmospheric oxalic acid and SOA production from glyoxal: Results of aqueous photooxidation  
573 experiments, *Atmos. Environ.*, 41, 7588-7602, <https://doi.org/10.1016/j.atmosenv.2007.05.035>,  
574 2007.

575 Chang, X., Zhao, B., Zheng, H., Wang, S., Cai, S., Guo, F., Gui, P., Huang, G., Wu, D., Han, L.,  
576 Xing, J., Man, H., Hu, R., Liang, C., Xu, Q., Qiu, X., Ding, D., Liu, K., Han, R., Robinson, A.  
577 L., and Donahue, N. M.: Full-volatility emission framework corrects missing and  
578 underestimated secondary organic aerosol sources, *One Earth*, 5, 403-412,  
579 <https://doi.org/10.1016/j.oneear.2022.03.015>, 2022.

580 Chen, Y., Guo, H., Nah, T., Tanner, D. J., Sullivan, A. P., Takeuchi, M., Gao, Z., Vasilakos, P., Russell,  
581 A. G., Baumann, K., Huey, L. G., Weber, R. J., and Ng, N. L.: Low-Molecular-Weight  
582 Carboxylic Acids in the Southeastern U.S.: Formation, Partitioning, and Implications for  
583 Organic Aerosol Aging, *Environ. Sci. Technol.*, 55, 6688-6699, 10.1021/acs.est.1c01413, 2021.

584 Dasari, S., Andersson, A., Bikkina, S., Holmstrand, H., Budhavant, K., Satheesh, S., Asmi, E., Kesti,  
585 J., Backman, J., Salam, A., Bisht, D. S., Tiwari, S., Hameed, Z., and Gustafsson, Ö.:  
586 Photochemical degradation affects the light absorption of water-soluble brown carbon in the  
587 South Asian outflow, *Sci. Adv.*, 5, eaau8066, 10.1126/sciadv.aau8066, 2019.

588 Elmquist, M., Cornelissen, G., Kukulska, Z., and Gustafsson, O.: Distinct oxidative stabilities of  
589 char versus soot black carbon: Implications for quantification and environmental recalcitrance,

590 Global Biogeochem. Cycles, 20, 10.1029/2005gb002629, 2006.

591 Ervens, B., Turpin, B. J., and Weber, R. J.: Secondary organic aerosol formation in cloud droplets  
592 and aqueous particles (aqSOA): a review of laboratory, field and model studies, *Atmos. Chem.*  
593 *Phys.*, 11, 11069-11102, 10.5194/acp-11-11069-2011, 2011.

594 Fang, W., Du, K., Andersson, A., Xing, Z., Cho, C., Kim, S.-W., Deng, J., and Gustafsson, Ö.: Dual-  
595 Isotope Constraints on Seasonally Resolved Source Fingerprinting of Black Carbon Aerosols  
596 in Sites of the Four Emission Hot Spot Regions of China, *J. Geophys. Res.: Atmos.*, 123,  
597 11,735-711,747, 10.1029/2018jd028607, 2018.

598 Fisseha, R., Spahn, H., Wegener, R., Hohaus, T., Brasse, G., Wissel, H., Tillmann, R., Wahner, A.,  
599 Koppmann, R., and Kiendler-Scharr, A.: Stable carbon isotope composition of secondary  
600 organic aerosol from  $\beta$ -pinene oxidation, *J. Geophys. Res.: Atmos.*, 114, 10.1029/2008jd011326,  
601 2009.

602 Fu, T.-M., Jacob, D. J., Wittrock, F., Burrows, J. P., Vrekoussis, M., and Henze, D. K.: Global  
603 budgets of atmospheric glyoxal and methylglyoxal, and implications for formation of secondary  
604 organic aerosols, *J. Geophys. Res.: Atmos.*, 113, 10.1029/2007jd009505, 2008.

605 Gkatzelis, G. I., Papanastasiou, D. K., Karydis, V. A., Hohaus, T., Liu, Y., Schmitt, S. H., Schlag, P.,  
606 Fuchs, H., Novelli, A., Chen, Q., Cheng, X., Broch, S., Dong, H., Holland, F., Li, X., Liu, Y.,  
607 Ma, X., Reimer, D., Rohrer, F., Shao, M., Tan, Z., Taraborrelli, D., Tillmann, R., Wang, H.,  
608 Wang, Y., Wu, Y., Wu, Z., Zeng, L., Zheng, J., Hu, M., Lu, K., Hofzumahaus, A., Zhang, Y.,  
609 Wahner, A., and Kiendler-Scharr, A.: Uptake of water-soluble gas-phase oxidation products  
610 drives organic particulate pollution in Beijing, *Geophys. Res. Lett.*, 48, e2020GL091351,  
611 <https://doi.org/10.1029/2020GL091351>, 2021.

612 Gustafsson, Ö., Kruså, M., Zencak, Z., Sheesley, R. J., Granat, L., Engström, E., Praveen, P. S., Rao,  
613 P. S. P., Leck, C., and Rodhe, H.: Brown Clouds over South Asia: Biomass or Fossil Fuel  
614 Combustion, *Science*, 323, 495-498, 10.1126/science.1164857, 2009.

615 Hallquist, M., Wenger, J. C., Baltensperger, U., Rudich, Y., Simpson, D., Claeys, M., Dommen, J.,  
616 Donahue, N. M., George, C., Goldstein, A. H., Hamilton, J. F., Herrmann, H., Hoffmann, T.,  
617 Iinuma, Y., Jang, M., Jenkin, M. E., Jimenez, J. L., Kiendler-Scharr, A., Maenhaut, W.,  
618 McFiggans, G., Mentel, T. F., Monod, A., Prevot, A. S. H., Seinfeld, J. H., Surratt, J. D.,  
619 Szmigielski, R., and Wildt, J.: The formation, properties and impact of secondary organic  
620 aerosol: current and emerging issues, *Atmos. Chem. Phys.*, 9, 5155-5236, 10.5194/acp-9-5155-  
621 2009, 2009.

622 Ho, K. F., Cao, J. J., Lee, S. C., Kawamura, K., Zhang, R. J., Chow, J. C., and Watson, J. G.:  
623 Dicarboxylic acids, ketocarboxylic acids, and dicarbonyls in the urban atmosphere of China, *J.*  
624 *Geophys. Res.: Atmos.*, 112, 10.1029/2006JD008011, 2007.

625 Ho, K. F., Lee, S. C., Cao, J. J., Kawamura, K., Watanabe, T., Cheng, Y., and Chow, J. C.:  
626 Dicarboxylic acids, ketocarboxylic acids and dicarbonyls in the urban roadside area of Hong  
627 Kong, *Atmos. Environ.*, 40, 3030-3040, 10.1016/j.atmosenv.2005.11.069, 2006.

628 Huang, L., Brook, J. R., Zhang, W., Li, S. M., Graham, L., Ernst, D., Chivulescu, A., and Lu, G.:  
629 Stable isotope measurements of carbon fractions (OC/EC) in airborne particulate: A new  
630 dimension for source characterization and apportionment, *Atmos. Environ.*, 40, 2690-2705,  
631 <https://doi.org/10.1016/j.atmosenv.2005.11.062>, 2006.

632 Huang, R.-J., Zhang, Y., Bozzetti, C., Ho, K.-F., Cao, J.-J., Han, Y., Daellenbach, K. R., Slowik, J.  
633 G., Platt, S. M., Canonaco, F., Zotter, P., Wolf, R., Pieber, S. M., Bruns, E. A., Crippa, M.,  
634 Ciarelli, G., Piazzalunga, A., Schwikowski, M., Abbaszade, G., Schnelle-Kreis, J.,  
635 Zimmermann, R., An, Z., Szidat, S., Baltensperger, U., El Haddad, I., and Prevot, A. S. H.: High  
636 secondary aerosol contribution to particulate pollution during haze events in China, *Nature*, 514,  
637 218-222, 10.1038/nature13774, 2014.

638 Huang, X.-F. and Yu, J. Z.: Is vehicle exhaust a significant primary source of oxalic acid in ambient  
639 aerosols?, *Geophys. Res. Lett.*, 34, 10.1029/2006gl028457, 2007.

640 Irei, S., Huang, L., Collin, F., Zhang, W., Hastie, D., and Rudolph, J.: Flow reactor studies of the  
641 stable carbon isotope composition of secondary particulate organic matter generated by OH-  
642 radical-induced reactions of toluene, *Atmos. Environ.*, 40, 5858-5867,  
643 <https://doi.org/10.1016/j.atmosenv.2006.05.001>, 2006.

644 Kawamura, K. and Bikkina, S.: A review of dicarboxylic acids and related compounds in  
645 atmospheric aerosols: Molecular distributions, sources and transformation, *Atmos. Res.*, 170,  
646 140-160, 10.1016/j.atmosres.2015.11.018, 2016.

647 Kawashima, H. and Haneishi, Y.: Effects of combustion emissions from the Eurasian continent in  
648 winter on seasonal  $\delta^{13}\text{C}$  of elemental carbon in aerosols in Japan, *Atmos. Environ.*, 46, 568-  
649 579, 10.1016/j.atmosenv.2011.05.015, 2012.

650 Kirillova, E. N., Sheesley, R. J., Andersson, A., and Gustafsson, Ö.: Natural abundance  $^{13}\text{C}$  and  
651  $^{14}\text{C}$  analysis of water-soluble organic carbon in atmospheric aerosols, *Anal. Chem.*, 82, 7973,  
652 2010.

653 Kirillova, E. N., Andersson, A., Han, J., Lee, M., and Gustafsson, Ö.: Sources and light absorption  
654 of water-soluble organic carbon aerosols in the outflow from northern China, *Atmos. Chem.*  
655 *Phys.*, 14, 1413-1422, 10.5194/acp-14-1413-2014, 2014a.

656 Kirillova, E. N., Andersson, A., Tiwari, S., Srivastava, A. K., Bisht, D. S., and Gustafsson, O.: Water-  
657 soluble organic carbon aerosols during a full New Delhi winter: Isotope-based source  
658 apportionment and optical properties, *J. Geophys. Res.: Atmos.*, 119, 3476-3485,  
659 10.1002/2013jd020041, 2014b.

660 Kirillova, E. N., Andersson, A., Sheesley, R. J., Kruså, M., Praveen, P. S., Budhavant, K., Safai, P.  
661 D., Rao, P. S. P., and Gustafsson, Ö.:  $^{13}\text{C}$ - and  $^{14}\text{C}$ -based study of sources and atmospheric  
662 processing of water-soluble organic carbon (WSOC) in South Asian aerosols, *J. Geophys. Res.:*  
663 *Atmos.*, 118, 614-626, 10.1002/jgrd.50130, 2013.

664 Lim, Y. B., Tan, Y., and Turpin, B. J.: Chemical insights, explicit chemistry, and yields of secondary  
665 organic aerosol from OH radical oxidation of methylglyoxal and glyoxal in the aqueous phase,  
666 *Atmos. Chem. Phys.*, 13, 8651-8667, 10.5194/acp-13-8651-2013, 2013.

667 Lim, Y. B., Tan, Y., Perri, M. J., Seitzinger, S. P., and Turpin, B. J.: Aqueous chemistry and its role  
668 in secondary organic aerosol (SOA) formation, *Atmos. Chem. Phys.*, 10, 10521-10539,  
669 10.5194/acp-10-10521-2010, 2010.

670 Link, M. F., Brophy, P., Fulgham, S. R., Murschell, T., and Farmer, D. K.: Isoprene versus  
671 Monoterpenes as Gas-Phase Organic Acid Precursors in the Atmosphere, *ACS Earth Space*  
672 *Chem.*, 5, 1600-1612, 10.1021/acsearthspacechem.1c00093, 2021.

673 Liu, D., Li, J., Cheng, Z., Zhong, G., Zhu, S., Ding, P., Shen, C., Tian, C., Chen, Y., Zhi, G., and

674 Zhang, G.: Sources of non-fossil-fuel emissions in carbonaceous aerosols during early winter  
675 in Chinese cities, *Atmos. Chem. Phys.*, 17, 11491-11502, 10.5194/acp-17-11491-2017, 2017.

676 Liu, D., Vonwiller, M., Li, J., Liu, J., Szidat, S., Zhang, Y., Tian, C., Chen, Y., Cheng, Z., Zhong, G.,  
677 Fu, P., and Zhang, G.: Fossil and Non-fossil Fuel Sources of Organic and Elemental  
678 Carbonaceous Aerosol in Beijing, Shanghai, and Guangzhou: Seasonal Carbon Source  
679 Variation, *Aerosol Air Qual. Res.*, 20, 2495-2506, 10.4209/aaqr.2019.12.0642, 2020.

680 Liu, J., Li, J., Liu, D., Ding, P., Shen, C., Mo, Y., Wang, X., Luo, C., Cheng, Z., Szidat, S., Zhang,  
681 Y., Chen, Y., and Zhang, G.: Source apportionment and dynamic changes of carbonaceous  
682 aerosols during the haze bloom-decay process in China based on radiocarbon and organic  
683 molecular tracers, *Atmos. Chem. Phys.*, 16, 2985-2996, 10.5194/acp-16-2985-2016, 2016a.

684 Liu, J., Li, J., Zhang, Y., Liu, D., Ding, P., Shen, C., Shen, K., He, Q., Ding, X., Wang, X., Chen, D.,  
685 Szidat, S., and Zhang, G.: Source apportionment using radiocarbon and organic tracers for  
686 PM<sub>2.5</sub> carbonaceous aerosols in Guangzhou, South China: contrasting local- and regional-scale  
687 haze events, *Environ. Sci. Technol.*, 48, 12002-12011, 10.1021/es503102w, 2014.

688 Liu, J., Li, J., Vonwiller, M., Liu, D., Cheng, H., Shen, K., Salazar, G., Agrios, K., Zhang, Y., He,  
689 Q., Ding, X., Zhong, G., Wang, X., Szidat, S., and Zhang, G.: The importance of non-fossil  
690 sources in carbonaceous aerosols in a megacity of central China during the 2013 winter haze  
691 episode: A source apportionment constrained by radiocarbon and organic tracers, *Atmos.*  
692 *Environ.*, 144, 60-68, 10.1016/j.atmosenv.2016.08.068, 2016b.

693 Lv, S., Wang, F., Wu, C., Chen, Y., Liu, S., Zhang, S., Li, D., Du, W., Zhang, F., Wang, H., Huang,  
694 C., Fu, Q., Duan, Y., and Wang, G.: Gas-to-Aerosol Phase Partitioning of Atmospheric Water-  
695 Soluble Organic Compounds at a Rural Site in China: An Enhancing Effect of NH<sub>3</sub> on SOA  
696 Formation, *Environ. Sci. Technol.*, 56, 3915-3924, 10.1021/acs.est.1c06855, 2022.

697 Martinelli, L. A., Camargo, P. B., Lara, L., Victoria, R. L., and Artaxo, P.: Stable carbon and nitrogen  
698 isotopic composition of bulk aerosol particles in a C<sub>4</sub> plant landscape of southeast Brazil, *Atmos.*  
699 *Environ.*, 36, 2427-2432, 10.1016/s1352-2310(01)00454-x, 2002.

700 Meng, J., Wang, G., Hou, Z., Liu, X., Wei, B., Wu, C., Cao, C., Wang, J., Li, J., Cao, J., Zhang, E.,  
701 Dong, J., Liu, J., Ge, S., and Xie, Y.: Molecular distribution and stable carbon isotopic  
702 compositions of dicarboxylic acids and related SOA from biogenic sources in the summertime  
703 atmosphere of Mt. Tai in the North China Plain, *Atmos. Chem. Phys.*, 18, 15069-15086,  
704 10.5194/acp-18-15069-2018, 2018.

705 Mo, Y., Li, J., Cheng, Z., Zhong, G., Zhu, S., Tian, C., Chen, Y., and Zhang, G.: Dual carbon isotope-  
706 based source apportionment and light absorption properties of water-soluble organic carbon in  
707 PM<sub>2.5</sub> over China, *J. Geophys. Res.: Atmos.*, e2020JD033920,  
708 <https://doi.org/10.1029/2020JD033920>, 2021.

709 Myriokefalitakis, S., Tsigaridis, K., Mihalopoulos, N., Sciare, J., Nenes, A., Kawamura, K., Segers,  
710 A., and Kanakidou, M.: In-cloud oxalate formation in the global troposphere: a 3-D modeling  
711 study, *Atmos. Chem. Phys.*, 11, 5761-5782, 10.5194/acp-11-5761-2011, 2011.

712 Pavuluri, C. M. and Kawamura, K.: Evidence for <sup>13</sup>-carbon enrichment in oxalic acid via iron  
713 catalyzed photolysis in aqueous phase, *Geophys. Res. Lett.*, 39, n/a-n/a, 10.1029/2011gl050398,  
714 2012.

715 Pavuluri, C. M., Kawamura, K., and Swaminathan, T.: Water-soluble organic carbon, dicarboxylic

716 acids, ketoacids, and  $\alpha$ -dicarbonyls in the tropical Indian aerosols, *J. Geophys. Res.: Atmos.*, 115,  
717 10.1029/2009jd012661, 2010.

718 Pavuluri, C. M., Kawamura, K., Swaminathan, T., and Tachibana, E.: Stable carbon isotopic  
719 compositions of total carbon, dicarboxylic acids and glyoxylic acid in the tropical Indian  
720 aerosols: Implications for sources and photochemical processing of organic aerosols, *J.*  
721 *Geophys. Res.: Atmos.*, 116, 10.1029/2011jd015617, 2011.

722 Qi, W., Wang, G., Dai, W., Liu, S., Zhang, T., Wu, C., Li, J., Shen, M., Guo, X., Meng, J., and Li,  
723 J.: Molecular characteristics and stable carbon isotope compositions of dicarboxylic acids and  
724 related compounds in wintertime aerosols of Northwest China, *Sci. Rep.*, 12, 11266,  
725 10.1038/s41598-022-15222-6, 2022.

726 Qiu, X., Duan, L., Chai, F., Wang, S., Yu, Q., and Wang, S.: Deriving High-Resolution Emission  
727 Inventory of Open Biomass Burning in China based on Satellite Observations, *Environ. Sci.*  
728 *Technol.*, 50, 11779-11786, 10.1021/acs.est.6b02705, 2016.

729 Shen, M., Ho, K. F., Dai, W., Liu, S., Zhang, T., Wang, Q., Meng, J., Chow, J. C., Watson, J. G.,  
730 Cao, J., and Li, J.: Distribution and stable carbon isotopic composition of dicarboxylic acids,  
731 ketocarboxylic acids and  $\alpha$ -dicarbonyls in fresh and aged biomass burning  
732 aerosols, *Atmos. Chem. Phys.*, 22, 7489-7504, 10.5194/acp-22-7489-2022, 2022.

733 Smith, B. N. and Epstein, S.: 2 categories of C-13/C-12 ratios for higher plants, *Plant Physiol.*, 47,  
734 380-8, 10.1104/pp.47.3.380, 1971.

735 Szidat, S., Jenk, T. M., Synal, H. A., Kalberer, M., Wacker, L., Hajdas, I., Kasper-Giebl, A., and  
736 Baltensperger, U.: Contributions of fossil fuel, biomass-burning, and biogenic emissions to  
737 carbonaceous aerosols in Zurich as traced by C-14, *J. Geophys. Res.: Atmos.*, 111,  
738 10.1029/2005jd006590, 2006.

739 Szidat, S., Jenk, T. M., Gaggeler, H. W., Synal, H. A., Fisseha, R., Baltensperger, U., Kalberer, M.,  
740 Samburova, V., Wacker, L., Saurer, M., Schwikowski, M., and Hajdas, I.: Source apportionment  
741 of aerosols by C-14 measurements in different carbonaceous particle fractions, *Radiocarbon*,  
742 46, 475-484, 10.1017/s0033822200039783, 2004.

743 van Pinxteren, D., Neusüß, C., and Herrmann, H.: On the abundance and source contributions of  
744 dicarboxylic acids in size-resolved aerosol particles at continental sites in central Europe, *Atmos.*  
745 *Chem. Phys.*, 14, 3913-3928, 10.5194/acp-14-3913-2014, 2014.

746 Wang, J., Wang, G., Wu, C., Li, J., Cao, C., Li, J., Xie, Y., Ge, S., Chen, J., Zeng, L., Zhu, T., Zhang,  
747 R., and Kawamura, K.: Enhanced aqueous-phase formation of secondary organic aerosols due  
748 to the regional biomass burning over North China Plain, *Environ. Pollut.*, 256, 113401,  
749 <https://doi.org/10.1016/j.envpol.2019.113401>, 2020.

750 Wang, J., Ye, J., Zhang, Q., Zhao, J., Wu, Y., Li, J., Liu, D., Li, W., Zhang, Y., Wu, C., Xie, C., Qin,  
751 Y., Lei, Y., Huang, X., Guo, J., Liu, P., Fu, P., Li, Y., Lee, H. C., Choi, H., Zhang, J., Liao, H.,  
752 Chen, M., Sun, Y., Ge, X., Martin, S. T., and Jacob, D. J.: Aqueous production of secondary  
753 organic aerosol from fossil-fuel emissions in winter Beijing haze, *Proc. Natl Acad. Sci. USA*,  
754 118, e2022179118, 10.1073/pnas.2022179118 %J Proceedings of the National Academy of  
755 Sciences, 2021.

756 Warneck, P.: In-cloud chemistry opens pathway to the formation of oxalic acid in the marine  
757 atmosphere, *Atmos. Environ.*, 37, 2423-2427, [https://doi.org/10.1016/S1352-2310\(03\)00136-5](https://doi.org/10.1016/S1352-2310(03)00136-5),

758 2003.

759 Widory, D., Roy, S., Le Moullec, Y., Goupil, G., Cocherie, A., and Guerrot, C.: The origin of  
760 atmospheric particles in Paris: a view through carbon and lead isotopes, *Atmos. Environ.*, 38,  
761 953-961, <https://doi.org/10.1016/j.atmosenv.2003.11.001>, 2004.

762 Wu, Z., Wang, Y., Tan, T., Zhu, Y., Li, M., Shang, D., Wang, H., Lu, K., Guo, S., Zeng, L., and  
763 Zhang, Y.: Aerosol liquid water driven by anthropogenic inorganic salts: implying its key role  
764 in haze formation over the North China Plain, *Environ. Sci. Technol. Lett.*, 5, 160-166,  
765 10.1021/acs.estlett.8b00021, 2018.

766 Xing, J., Lu, X., Wang, S., Wang, T., Ding, D., Yu, S., Shindell, D., Ou, Y., Morawska, L., Li, S.,  
767 Ren, L., Zhang, Y., Loughlin, D., Zheng, H., Zhao, B., Liu, S., Smith, K. R., and Hao, J.: The  
768 quest for improved air quality may push China to continue its CO<sub>2</sub> reduction beyond the Paris  
769 Commitment, *Proc. Natl Acad. Sci. USA*, 117, 29535-29542, 10.1073/pnas.2013297117, 2020.

770 Xu, B., Cheng, Z., Gustafsson, Ö., Kawamura, K., Jin, B., Zhu, S., Tang, T., Zhang, B., Li, J., and  
771 Zhang, G.: Compound-specific radiocarbon analysis of low molecular weight dicarboxylic  
772 acids in ambient aerosols using preparative gas chromatography: method development, *Environ.*  
773 *Sci. Technol. Lett.*, 8, 135-141, 10.1021/acs.estlett.0c00887, 2021.

774 Xu, B., Zhang, G., Gustafsson, Ö., Kawamura, K., Li, J., Andersson, A., Bikkina, S., Kunwar, B.,  
775 Pokhrel, A., Zhong, G., Zhao, S., Li, J., Huang, C., Cheng, Z., Zhu, S., Peng, P., and Sheng, G.:  
776 Large contribution of fossil-derived components to aqueous secondary organic aerosols in  
777 China, *Nat. Commun.*, 13, 5115, 10.1038/s41467-022-32863-3, 2022.

778 Yu, Q., Chen, J., Cheng, S., Qin, W., Zhang, Y., Sun, Y., and Ahmad, M.: Seasonal variation of  
779 dicarboxylic acids in PM<sub>2.5</sub> in Beijing: Implications for the formation and aging processes of  
780 secondary organic aerosols, *Sci. Total Environ.*, 763, 142964,  
781 <https://doi.org/10.1016/j.scitotenv.2020.142964>, 2021.

782 Zhang, G., Liu, J., Li, J., Li, P., Wei, N., and Xu, B.: Radiocarbon isotope technique as a powerful  
783 tool in tracking anthropogenic emissions of carbonaceous air pollutants and greenhouse gases:  
784 A review, *Fundam. Res.*, 1, 306-316, <https://doi.org/10.1016/j.fmre.2021.03.007>, 2021.

785 Zhang, Y.-L., Kawamura, K., Cao, F., and Lee, M.: Stable carbon isotopic compositions of low-  
786 molecular-weight dicarboxylic acids, oxocarboxylic acids,  $\alpha$ -dicarbonyls, and fatty acids:  
787 Implications for atmospheric processing of organic aerosols, *J. Geophys. Res.: Atmos.*, 121,  
788 3707-3717, 10.1002/2015jd024081, 2016.

789 Zhang, Y.-L., Schnelle-Kreis, J., Abbaszade, G., Zimmermann, R., Zotter, P., Shen, R.-r., Schaefer,  
790 K., Shao, L., Prevot, A. S. H., and Szidat, S.: Source Apportionment of Elemental Carbon in  
791 Beijing, China: Insights from Radiocarbon and Organic Marker Measurements, *Environ. Sci.*  
792 *Technol.*, 49, 8408-8415, 10.1021/acs.est.5b01944, 2015.

793 Zhang, Y., Ren, H., Sun, Y., Cao, F., Chang, Y., Liu, S., Lee, X., Agrios, K., Kawamura, K., Liu, D.,  
794 Ren, L., Du, W., Wang, Z., Prévôt, A. S. H., Szidat, S., and Fu, P.: High Contribution of  
795 Nonfossil Sources to Submicrometer Organic Aerosols in Beijing, China, *Environ. Sci. Technol.*,  
796 51, 7842-7852, 10.1021/acs.est.7b01517, 2017.

797 Zhao, B., Zheng, H., Wang, S., Smith, K. R., Lu, X., Aunan, K., Gu, Y., Wang, Y., Ding, D., Xing,  
798 J., Fu, X., Yang, X., Liou, K.-N., and Hao, J.: Change in household fuels dominates the decrease  
799 in PM<sub>2.5</sub> exposure and premature mortality in China in 2005–2015, *Proc. Natl*



800 Acad. Sci. USA, 115, 12401-12406, 10.1073/pnas.1812955115 %J Proceedings of the National  
801 Academy of Sciences, 2018.  
802 Zhao, S., Tian, L., Zou, Z., Liu, X., Zhong, G., Mo, Y., Wang, Y., Tian, Y., Li, J., Guo, H., and Zhang,  
803 G.: Probing Legacy and Alternative Flame Retardants in the Air of Chinese Cities, Environ. Sci.  
804 Technol., 10.1021/acs.est.0c07367, 2021.  
805 Zhu, S., Ding, P., Wang, N., Shen, C., Jia, G., and Zhang, G.: The compact AMS facility at  
806 Guangzhou Institute of Geochemistry, Chinese Academy of Sciences, Nucl. Instrum. Methods  
807 Phys. Res., Sect. B, 361, 72-75, 10.1016/j.nimb.2015.06.040, 2015.  
808